# Quantum-Accelerated Solution of Nonlinear Equations from Variational Principles

Katsuhiro Endo\* and Kazuaki Z. Takahashi<sup>†</sup>
National Institute of Advanced Industrial Science and Technology (AIST),
Materials DX Research Center,
Central 2, 1-1-1 Umezono,
Tsukuba, Ibaraki 305-8568, Japan
(Dated: August 26, 2025)

The variational principle serves as a fundamental framework for describing equilibrium states of physical systems via the minimization or extremization of an energy-like functional. While quantum algorithms have demonstrated promising advances in efficiently solving linear problems rooted in this principle, extending these techniques to nonlinear equilibrium equations—ubiquitous in structural mechanics, fluid dynamics, and electromagnetism—remains an outstanding challenge. Here, we introduce a novel algorithm tailored for fault-tolerant quantum computers (FTQCs) that directly addresses nonlinear equilibrium conditions governed by the variational principle. Our approach recasts the static nonlinear problem as a time-evolution process, enabling an effective linearization amenable to quantum acceleration. This construction permits quantum acceleration of nonlinear equilibrium computations on FTQCs. Compared to classical solvers, our method offers significant memory savings without compromising accuracy, with computational complexity scaling linearly in simulation time and independent of system size. We validate the algorithm through accurate prediction of nonlinear deformation in springs and truss systems, demonstrating its potential for scalable quantum acceleration of nonlinear physical phenomena. This work paves the way toward leveraging fault-tolerant quantum computing for complex nonlinear systems across physics and engineering disciplines.

### I. INTRODUCTION

The variational principle—most prominently expressed as the principle of least action—is a foundational and unifying concept in theoretical physics. It provides a systematic and elegant framework for describing the dynamics of a broad class of physical systems, from classical mechanics[1] to quantum field theory[2] and general relativity[3]. By formulating physical laws as the extremization of an action integral, it yields the governing equations of motion and reveals deep connections between symmetries and conservation laws via Noether's theorem[4]. This formulation is remarkably general: it applies to both discrete and continuous systems and bridges classical and quantum descriptions—most notably through the path integral formalism.

Beyond fundamental physics, the variational principle underpins many classical theories through the extremization of energy- or entropy-based functionals. In solid mechanics, the principle of minimum potential energy governs the equilibrium of elastic structures and forms the basis of numerical methods such as the finite element method[5]. Fluid dynamics derives the Euler equations for ideal flows from Hamilton's principle[6]. Electromagnetic theory expresses Maxwell's equations through a variational formalism involving the electromagnetic field tensor and Lagrangian density[7]. In thermodynamics and statistical mechanics, maximizing entropy yields equilibrium distributions such as the Gibbs ensemble[8].

These diverse applications demonstrate the principle's versatility in capturing nonlinear phenomena, including large deformations, turbulent flows, nonlinear wave propagation, and temperature-dependent transport.

Solving the nonlinear equations that arise from these variational formulations typically relies on classical computing. Sophisticated numerical techniques—including nonlinear finite element analysis, Newton-Raphson solvers, and multiscale methods—enable high-fidelity simulations of complex physical systems[9]. However, in strongly nonlinear regimes, classical approaches face persistent challenges such as high computational cost, convergence failure, sensitivity to parameters, and the presence of bifurcations or stochastic effects [10, 11]. These limitations have motivated the exploration of emerging computational strategies such as reduced-order modeling, uncertainty quantification, and quantum computing.

Fault-tolerant quantum computers (FTQCs) are anticipated to offer computational advantages for problems intractable on classical machines. Following early breakthroughs like Shor's and Grover's algorithms[12, 13], recent efforts have explored quantum acceleration of classical simulations, particularly for linear differential equations such as the heat and wave equations[14, 15]. These results suggest that FTQCs could become powerful tools in simulation-driven science and engineering.

Quantum acceleration algorithms can be broadly categorized along two axes: equilibrium vs. dynamical analysis, and linear vs. nonlinear systems. For linear equilibrium problems, a variety of quantum linear system solvers (QLSAs) have been developed, including the HHL algorithm[16], quantum singular value transformation (QSVT)[17], and adiabatic methods[18, 19]. These have been applied to systems arising from finite element

<sup>\*</sup> katsuhiro.endo@aist.go.jp

<sup>†</sup> kazu.takahashi@aist.go.jp

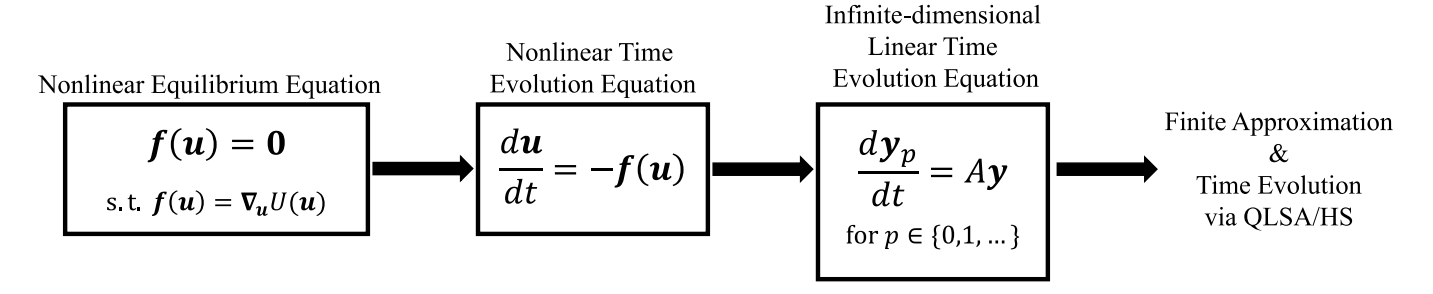


FIG. 1. Flowchart of our proposed method for transforming a nonlinear equilibrium equation into a linear system solvable by quantum algorithms. The nonlinear equilibrium equation is first reformulated as a nonlinear time evolution equation, which is then rigorously linearized (e.g., by Carleman linearization or PSC method) into an infinite-dimensional system. A finite-dimensional approximation is subsequently applied, allowing the problem to be solvable using QLSA or HS.

discretizations[20] and electromagnetic simulations[21]. To address scaling issues related to large condition numbers, quantum preconditioning techniques have been introduced, as demonstrated by Clader et al[22]. For linear dynamical systems, both QLSA-based[23, 24] and Hamiltonian simulation (HS)-based[15, 25–28] approaches have been proposed. Babbush et al. demonstrated exponential quantum advantage in simulating large-scale coupled oscillator systems via HS[29]. Moreover, several studies have extended HS to non-unitary dynamics using techniques such as unitary dilation[30], warped phase transformations[31], and linear combination of unitaries[32, 33].

In contrast, quantum algorithms for nonlinear problems remain relatively underdeveloped. For nonlinear dynamical systems, Carleman and Koopman-von Neumann linearization techniques[34–40] have been proposed to embed nonlinear evolution into high-dimensional linear systems, which can then be addressed by QLSAs. Liu et al. showed that second-order nonlinear systems can be simulated in this way[34]. Our prior work introduced the Pivot Switching Carleman method[41], which improves numerical stability and extends applicability to strongly nonlinear systems, including phase-field models.

For nonlinear equilibrium problems, only a few approaches exist. Xue et al. proposed a homotopy perturbation method to reduce quadratic nonlinearities to linear form, achieving exponential speedup in state dimension[42]. Nghiem et al. developed a quantum version of Newton's method based on block-encoded arithmetic oracles, capable of solving general homogeneous nonlinear equations, though it requires exponentially many oracle queries with respect to the steps[43]. Despite these promising directions, practical applications to real-world nonlinear systems remain scarce and largely unvalidated.

In this study, we propose a novel quantum algorithm for solving nonlinear equilibrium equations derived from variational principles. Targeting systems governed by balance of forces, our approach reformulates the equilibrium condition as a nonlinear dynamical system. By applying exact linearization method to the resulting infinite

dimensional time-evolution equations, we reconstruct the solution to the original nonlinear equilibrium problem. This formulation enables, for the first time, quantum acceleration of structurally nonlinear equilibrium analyses using fault-tolerant quantum computers. As demonstrated in the following sections, the proposed approach opens a path toward practical quantum accelerations in structural mechanics.

#### II. METHOD

In this section, we state the setting of our target problem and describe our simple method to solve nonlinear equilibrium equations.

#### A. Problem Statement

Let  $\boldsymbol{u}=(u_1,u_2,\cdots,u_D)\in\mathbb{R}^D$  be a state vector of the system, and let  $\boldsymbol{f}(\cdot):\mathbb{R}^D\to\mathbb{R}^D$  be a system-specific vector-valued nonlinear functions. We consider the problem of finding an equilibrium point  $\boldsymbol{u}^*$  that satisfies the equilibrium equations

$$f(u^*) = 0. (1)$$

In the variational principle, the equilibrium equations always have a variational form, that is, there exists a scalar-valued potential function  $U(\cdot): \mathbb{R}^D \to \mathbb{R}$  satisfies

$$f(u) = \nabla_{u} U(u). \tag{2}$$

To avoid instability, we assume U satisfies the following two conditions: (1)  $\nabla_{\boldsymbol{u}}U$  is locally Lipschitz continuous in anywhere, (2)  $U(\boldsymbol{u}) \to \infty$  when  $\|\boldsymbol{u}\| \to \infty$ . Our proposed method aims to find any one of  $\boldsymbol{u}^*$  that satisfies Eq. (1), given a nonlinear function  $\boldsymbol{f}$  satisfies above conditions.

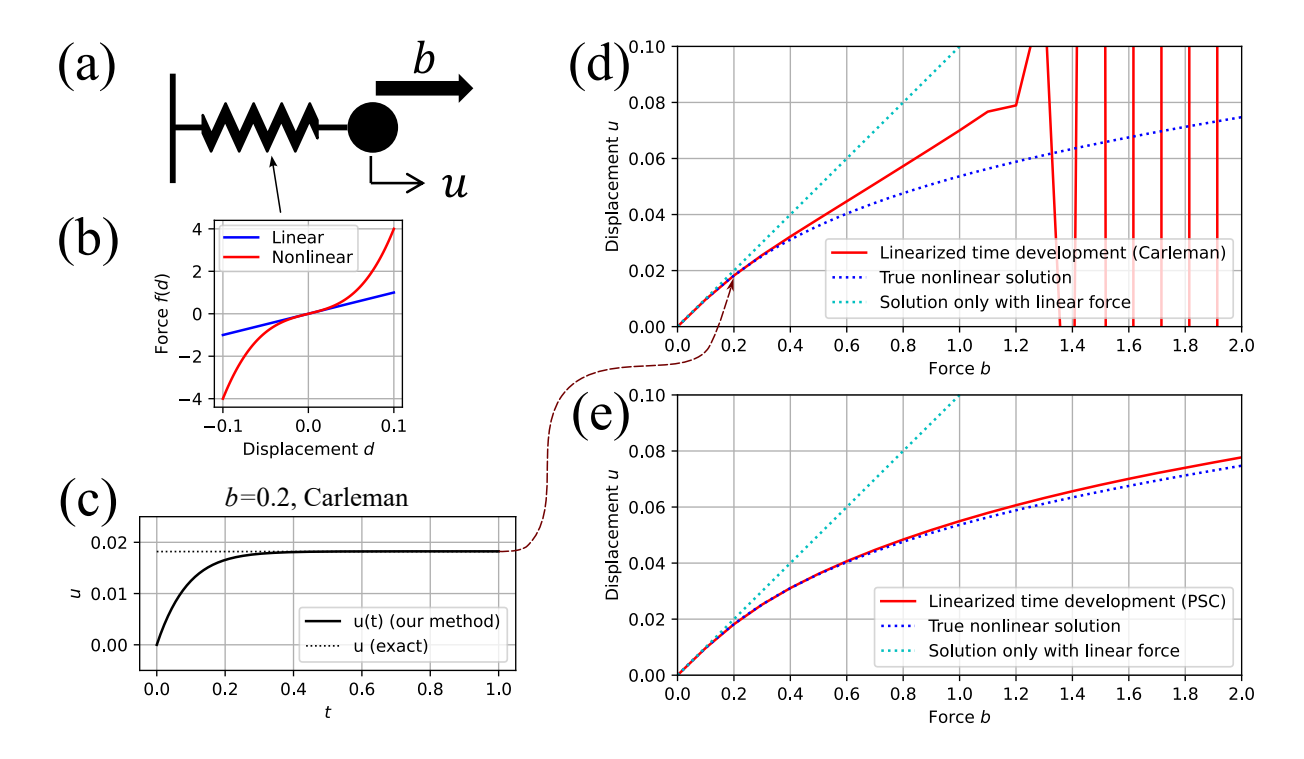


FIG. 2. Results for a one-dimensional single nonlinear spring system. (a) Target spring-mass system. (b) Force-displacement relations for the nonlinear spring k = 10, a = 3000 (red) and k = 10, a = 0 (blue). (c) Example of the time evolution of the displacement u obtained by our method, converging to the correct solution. (d) Obtained displacement using our method with Carleman linearization for each strength of the external force (red). Exact solution (blue dashed) and the linear-spring case (light-blue dashed) are included for comparison. (e) Obtained displacement using our method with PSC linearization.

#### B. Proposed Method

To solve nonlinear equilibrium equations in Eq. (1), we consider the following time evolution equations

$$\frac{d\boldsymbol{u}}{dt} = -\boldsymbol{f}(\boldsymbol{u}). \tag{3}$$

Starting from any initial state u(0) and solving the above time evolution equation, u(t) always reach a state that satisfies Eq. (1) as  $t \to \infty$  (a simple proof is given in Appendix A). This means that, rather than solving nonlinear equilibrium equations in Eq. (1) directly, we solve the equations to perform the time evolution that follows Eq. (3).

Since Eq. (3) is generally nonlinear, we can use exact linearization technique to transform nonlinear time evolution equations into infinite dimensional linear time evolution equations such as Carleman linearization and Koopman von Neumann linearization. It should be noted that these linearization methods cannot be directly applied to nonlinear equations without time dependence, such as Eq. (1). Therefore, converting it to a time-dependent form like Eq. (3) is the simple but key point of our proposed method. Then, by truncating the resulting infinite-dimensional linear equations to a finite dimension, efficient linear dynamical simulations can be performed using methods such as QLSA and HS, as de-

scribed in the introduction section. Fig. 1 shows the flowchart for our proposed method described above.

## III. EXAMPLES AND NUMERICAL RESULTS

In this section, we show the applicability of our method by solving three specific problems in the field of non-linear elasticity. First, we examine the simplest nonlinear system, a single-point nonlinear spring model. We formulated truncated linearized time evolution equations derived from our proposed method and verified the numerical results of its dynamics simulation. Second, we evaluate the computational cost of our method for a one-dimensional multi-mass nonlinear spring model. We also show the numerical simulation results under specific conditions on the second model. Third, we demonstrate the extensibility of our method by solving the small two-dimensional truss problems.

# A. one-dimensional single nonlinear spring

We consider a one-dimensional space in which a fixed point A located in x = -1 and a point mass B located in x = u are connected by a single spring, as shown in Fig. 2(a). The spring has a natural length of 1, and its

force of restoring f(d) with respect to the spring displacement d is given by

$$f(d) = kd + ad^3, (4)$$

where k > 0,  $a \ge 0$  characterize the spring properties. Fig. 2(b) shows this force-displacement relationship, which indicates that this spring is made of nonlinear hyper-elastic material.

When an external force  $b \ge 0$  is applied to the point mass B, we got the equilibrium equations of external force and internal spring forces:

$$ku + au^3 - b = 0, (5)$$

which is the equation to solve. This equation contains a cubic term for the unknown variable u, thus classifying it as a nonlinear equilibrium equation.

To use our proposed method, we can find the scalar potential

$$U(u) := \frac{1}{2}ku^2 + \frac{1}{4}au^4 - bu, \tag{6}$$

which satisfies the relation

$$ku + au^3 - b = \nabla_u U(u). \tag{7}$$

This relationship can be derived from the fact that U is the total potential energy, or the sum of the internal potential energy of the spring and the work done by the external force. Based on the principle of stationary potential energy—it is one of the type of variational principle—, the system must exist at stationary point  $(\nabla_u U = 0)$  in equilibrium.

The potential U satisfies the conditions required for our proposed method: any multivariate polynomial function is locally Lipschitz continuous and U(d) approaches infinite as  $|u| \to \infty$ .

Therefore, using our method, the nonlinear equilibrium equation Eq. (5) can be transformed into the following nonlinear time evolution equations

$$\frac{du}{dt} = -ku - au^3 + b. (8)$$

The implementation of this time evolution on a quantum computer is achieved through the utilization of exact linearization to the infinite dimensional linear dynamics. In Carleman linearization, an infinite number of variable, denoted by  $y_p = u^p \ (p \in \mathbb{N} \cup \{0\})$  are introduced. The time derivative of  $y_p$  results in the dynamics of the infinite-dimensional system

$$\frac{dy_p}{dt} = p(-ky_p - ay_{p+2} + by_{p-1}). \tag{9}$$

Clearly, the resulting equation is a linear time evolution equation. Truncating all terms  $p > P \in \mathbb{Z}$  yields a

truncated finite-dimensional linear time evolution equations. For example, in P=5 case this can be written in matrix form as

$$\frac{d}{dt} \begin{bmatrix} y_0 \\ y_1 \\ y_2 \\ y_3 \\ y_4 \\ y_5 \end{bmatrix} = \begin{bmatrix} 0 & 0 & 0 & 0 & 0 & 0 \\ b & -k & 0 & -a & 0 & 0 \\ 0 & 2b & -2k & 0 & -2a & 0 \\ 0 & 0 & 3b & -3k & 0 & -3a \\ 0 & 0 & 0 & 4b & -4k & 0 \\ 0 & 0 & 0 & 0 & 5b & -5k \end{bmatrix} \begin{bmatrix} y_0 \\ y_1 \\ y_2 \\ y_3 \\ y_4 \\ y_5 \end{bmatrix}, (10)$$

and this time evolution equation can be simulated using well known quantum algorithms such as QSLA and HS.

Next, we will verify the solution to the nonlinear equilibrium equation obtained by solving the above linear time evolution. We numerically integrated Eq. (10) and got the value of  $y_1(t = T_{end})$  for each external force  $b = 0.0, 0.1, \dots, 2.0$ . We used  $T_{\rm end} = 1$  as sufficiently large time length. We also used the spring properties k = 10 and a = 3000 in the numerical simulation results. As the initial value of the state, u(t = 0) = 0 was set as the natural state with no external force. Fig. 2(c) shows an example of the time evolution trajectory of  $y_1(t)$  at b=0.2. In Fig. 2(d), the red line shows the  $y_1(t=T_{\rm end})$ as a solution of Eq. (5) based on our method and Carleman Linearization. The blue dotted line shows the exact solution of Eq. (5). Additionally, the light-blue line shows the exact solution for linear spring case where we set k = 10, a = 0 in Eq. (5).

Fig. 2(d) indicates that the use of our method with Carleman linearization successfully replicates the exact solution up to a limit of b < 0.3. Even in this range of b, both the region where the nonlinear spring behaves like linear spring ( $b \leq 0.1$ ) and the region where the nonlinearity of the spring appears and the spring displacement is suppressed compared to that of the linear spring (0.1 < b < 0.3) can be correctly solved. This means that our proposed method can solve nonlinear equilibrium equation beyond the range of linearity.

Conversely, for  $b \geq 0.3$ , the error increases in proportion to the rise in b. For  $b \geq 1.2$ , the time evolution diverged. Eigenvalue analysis of system matrix in Eq. (10) reveals that its real parts become positive for b > 1.145. Linear dynamics with positive eigenvalues always diverge, so the solution are essentially invalid for b in this range. We also confirmed that this behavior persists even if the truncation degree P in greatly increased.

In fact, such divergence problems have been reported in previous studies employing Carleman linearization [44–46]. To improve this problem, our earlier work proposed the Pivot Switching Carleman (PSC) linearization[41], which shifts the pivot state s in the polynomial expansion. For pivot state  $s \in \mathbb{R}$  and the truncation order P=5, the PSC-linearized dynamical system takes the form

$$\frac{d}{dt} \begin{bmatrix} y_0 \\ y_1 \\ y_2 \\ y_3 \\ y_4 \\ y_5 \end{bmatrix} = \begin{bmatrix} 0 & 0 & 0 & 0 & 0 & 0 & 0 \\ b & -k & 0 & -a & 0 & 0 \\ 0 & 2b & -2k & 0 & -2a & 0 \\ 0 & 0 & 3b & -3k & 0 & -3a \\ 4as^6 & -24s^5 & 60as^3 & -4k + 80as^3 & -4k + 60as^2 & -24as \\ 30as^2 & -175as^6 & 420as^5 & -525as^4 & 5b + 350as^3 & -5k - 105as^2 \end{bmatrix} \begin{bmatrix} y_0 \\ y_1 \\ y_2 \\ y_3 \\ y_4 \\ y_5 \end{bmatrix}.$$
(11)

One can see that only coefficients of the bottom two rows, which associated with the time evolution of two highest orders variables  $\{y_4, y_5\}$ , differ from the Carleman linearized matrix in Eq. (10). This is because the PSC method can be regarded as adjusting the finite-dimensional truncation with respect to Carleman linearization.

Note that the PSC method requires selecting an appropriate pivot state. Prior work suggested that the pivot state should be as close to the current state as possible. In our case, while the sign of u(t) is always expected to be positive because the sign of the external force is positive, the value of u(t) itself cannot be determined before the simulations. Thus we set s=0.01, a small positive value that can be chosen without any a prior analysis. Alternatively, if we can simulate the time evolution equation using classical methods when the nonlinear terms are ignored, the pivot state can be determined from such simulation results. There is room for improvement in determining the appropriate pivot state according to the nature of the problem.

Fig. 2(e) shows the simulation results based on our proposed method and PSC linearization. Unlike Carleman linearization, the obtained solution using the PSC method maintains convergence even when  $b \geq 1.2$ , and agrees closely with the exact solution for all b. This fact means that the performance of our proposed method can be improved by appropriately selecting a exact linearization method for the obtained nonlinear time evolutions.

#### B. one-dimensional chain of nonlinear springs

We next consider a one-dimensional chain of multiple masses as shown in Fig. 3(a). Let the number of point masses be N. The i-th mass is located at  $x = i + u_i$ , where  $u_i$  denotes its displacement from the natural position. We imposed periodic boundary conditions with the length N, and connect all adjacent masses with identical nonlinear springs governed by Eq. (4). All springs are at their natural length when  $u_i = 0$ , so the natural length of all springs is 1.

Let external forces  $\mathbf{b} = (b_0, b_1, \dots, b_{N-1})$  act on each mass. Our goal is to find the equilibrium displacement  $\mathbf{u} = (u_0, u_1, \dots, u_{N-1})$ . As in the previous section, the

total potential energy of this system can be written as

$$U_{\text{int}}(\boldsymbol{u}) = \sum_{i=0}^{N-1} \left[ \frac{1}{2} k(u_i - u_{i+1})^2 + \frac{1}{4} a(u_i - u_{i+1})^4 + b_i u_i \right],$$
(12)

where we use the notation  $u_N = u_0$ . Thus the time evolution equations which yields the equilibrium state is

$$\frac{du_i}{dt} = -k \left[ (u_i - u_{i-1}) + (u_i - u_{i-1}) \right] - a \left[ (u_i - u_{i-1})^3 + (u_i - u_{i-1})^3 \right] + b_i$$
 (13)

for all i.

For ease of subsequent analysis, we rewrite Eq. (13) as

$$\frac{d\mathbf{u}}{dt} = F_0 \mathbf{u}^{\otimes 0} + F_1 \mathbf{u}^{\otimes 1} + F_3 \mathbf{u}^{\otimes 3} \tag{14}$$

where

$$F_0 = [\boldsymbol{b}] \in \mathbb{R}^{N \times 1},\tag{15}$$

$$F_1 = k(S + S^T - 2I) \in \mathbb{R}^{N \times N},\tag{16}$$

$$F_3 = aV \{ (S^T - I)^{\otimes 3} - (I - S)^{\otimes 3} \} \in \mathbb{R}^{N \times N}.$$
 (17)

Here we use the cyclic shift matrix S defines as  $(S\boldsymbol{u})_i = u_{i+1}$ , or equivalently,  $(S^T\boldsymbol{u})_i = u_{i-1}$ , and the special projector matrix V defined as  $(V\boldsymbol{u}^{\otimes 3})_i = u_i^3$ . The equivalence of Eq. (13) and Eq. (14) is shown in Appendix B.

Next we apply Carleman linearization. Let introduce the variables  $y_p = u^{\otimes p}$ . Taking the time derivative of the variables  $y_p$ , we get the following infinite-dimensional linear time-evolution equation

$$\frac{d\mathbf{y}_p}{dt} = C(F_0, p)\mathbf{y}_{p-1} + C(F_1, p)\mathbf{y}_p + C(F_3, p)\mathbf{y}_{p+2},$$
(18)

where we defined the matrix-valued function

$$C(F,p) = \sum_{v=0}^{p-1} \underbrace{I \otimes \cdots \otimes I}_{v \text{ times}} \otimes F \otimes \underbrace{I \otimes \cdots \otimes I}_{p-1-v \text{ times}}.$$
(19)

For example, truncating this time-evolution equation at order P=5 gives

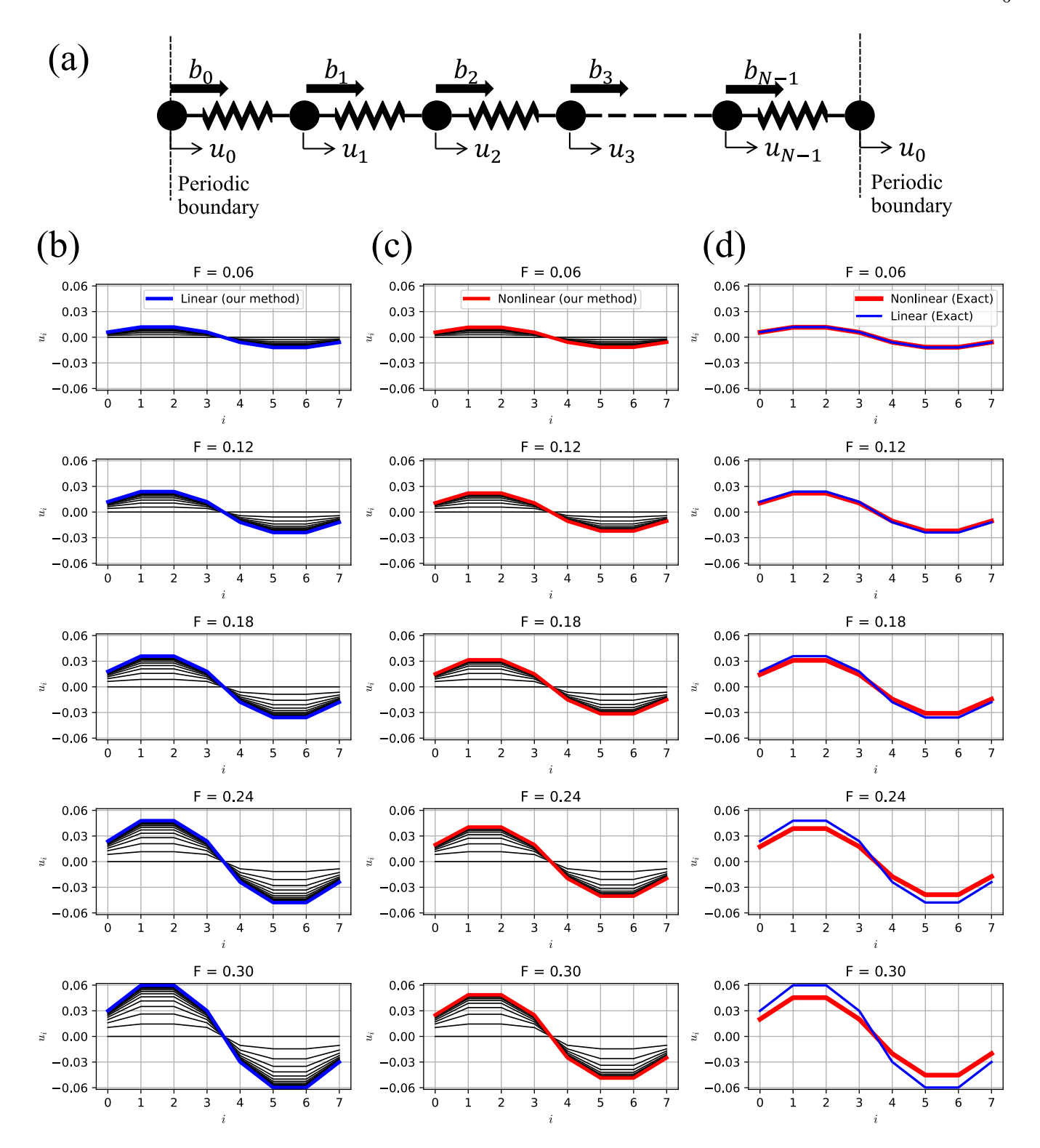


FIG. 3. Results for a one-dimensional nonlinear chain-spring system. (a) Target chain-spring system with periodic boundary conditions. (b) Obtained displacements using our method with Carleman linearization for the linear spring case (blue). Intermediate trajectories are also plotted (black). (c) Obtained displacements using our method with Carleman linearization for the nonlinear spring case (red). (d) Exact solution for linear spring (blue) and nonlinear spring (red).

$$\frac{d}{dt} \begin{bmatrix} y_0 \\ y_1 \\ y_2 \\ y_3 \\ y_4 \\ y_5 \end{bmatrix} = \begin{bmatrix}
O & O & O & O & O \\
C(F_0, 1) & C(F_1, 1) & O & C(F_3, 1) & O & O \\
O & C(F_0, 2) & C(F_1, 2) & O & C(F_3, 2) & O \\
O & O & C(F_0, 3) & C(F_1, 3) & O & C(F_3, 3) \\
O & O & O & C(F_0, 4) & C(F_1, 4) & O \\
O & O & O & O & C(F_0, 5) & C(F_1, 5)
\end{bmatrix} \begin{bmatrix} y_0 \\ y_1 \\ y_2 \\ y_3 \\ y_4 \\ y_5 \end{bmatrix},$$
(20)

where O denotes a zero matrix.

To evaluate the effectiveness of this linearization, we performed classical numerical simulations of Eq. (20). We use the number of mass N=8, and the same spring parameters as in the previous section: k=10, a=3000. As a external forces, we applied +F on the left half of the chain and -F on the right half of the chain, or

$$b_0 = b_1 = b_2 = b_3 = F, \ b_4 = b_5 = b_6 = b_7 = -F, \ (21)$$

where we performed simulations for different value of F from 0.00 to 0.30. We then obtained the numerically integrated results of Eq. (20) on t = 1.

The simulation results are shown as the red curves in Fig. 3(c). In this figure, the displacement of the mass  $u_i$  indexed by the number i on the horizontal axis is plotted on the vertical axis. The black lines shows the transient behavior of the states up to t=1. For comparison, the red curves in Fig. 3(d) show the exact solution obtained by directly solving the nonlinear equilibrium equations  $\nabla_u U(u) = 0$  using the classical solver. In addition, we add the the same simulation results except for using the linear springs (i.e. k=10, a=0). For linear case, the blue curves in Fig. 3(b) is the results obtained by our method, and the blue curves in Fig. 3(d) is the exact solutions obtained by the classical solver.

The results obtained by our method (red in Fig. 3(c)) agree with the exact nonlinear solution (red in Fig. 3(d)) for all F. Comparing the nonlinear (red) and linear (blue) results of the exact simulation in Fig. 3(d), the responses are nearly identical up to F=1.2, indicating spring nonlinearity appears beyond this range. The obtained results using our method (Fig. 3(c)) also accurately reproduce these transition from linear to nonlinear, demonstrating that our method is also effective for this nonlinear chain system.

We can also estimate the query complexity to simulate truncated linearized dynamics for this chain system in general N and P. As a generalization of Eq. (20), we can write Carleman-linearized time evolution equation

$$\frac{d\mathbf{y}}{dt} = A\mathbf{y},\tag{22}$$

where  $\mathbf{y} = (\mathbf{y}_0, \cdots, \mathbf{y}_P)^T$  and (i, j)-block of A is  $C(F_{j-i+1}, i)$  for i > 0 and  $j - i + 1 \in \{0, 1, 3\}$ , and is zero matrix for the other case  $(0 \leq i, j \leq P)$ . Earlier studies on the Hamiltonian simulation suggested that, given the block encoding of  $A/\alpha$ , the query complexity

for simulating Eq. (22) grows as  $\mathcal{O}(\alpha t + \ln(1/\epsilon))[47, 48]$ . Here  $\alpha$  is scaling factor to embed the matrix A into the block-encoding unitary matrix, t is the length of time evolution, and  $\epsilon$  is the target error. In best case, the scaling factor can be selected to  $\alpha = ||A||_2$ . This makes the query complexity to simulate Eq. (22) on quantum computer as

$$\mathcal{O}(P^{3/2}(\|\mathbf{b}\| + k + a)t + \ln(1/\epsilon)).$$
 (23)

Appendix C shows the proof of the above estimation.

This analysis reveals that the query complexity scales linearly with respective to the norm of the external force  $\|\boldsymbol{b}\|$ , linear and nonlinear coefficient of the spring k, a, the truncation order to the power of two-thirds  $P^{3/2}$ . When the external force vector  $\boldsymbol{b}$  is sparse vector, the norm is approximately constant. The coefficients k and a, as well as the truncation order P, are also constant. Thus the query complexity of this time evolution is not depends on the number of masses N for any t. Note that further investigation is required to estimate preferred length of time evolution t.

We can also estimate the required number of qubits. Assume that additional ancilla qubits required for the block-encoding of  $A/\alpha$  and for the Hamiltonian simulation are constant with respect to N. Since the dimension of y is

$$\dim(\mathbf{y}) = \sum_{p=1}^{P} N^p \le 2N^P = 2^{1+P\log_2 N},$$
 (24)

so the required number of qubits scales as  $\mathcal{O}(P\log N)$ . In other words, we only require logarithmically number of quantum bits with respect to the size of the system N, indicating the quantum advantage over classical computers.

#### C. two-dimensional nonlinear truss structure

As a final example, we consider a two-dimensional truss composed of nonlinear spring elements, as shown in Fig. 4(a). This example demonstrates that our method can be applied to more practical systems.

Consider there exists N point masses on a twodimensional space, connected by nonlinear springs between the two masses  $(i, j) \in G$  in the set G. When

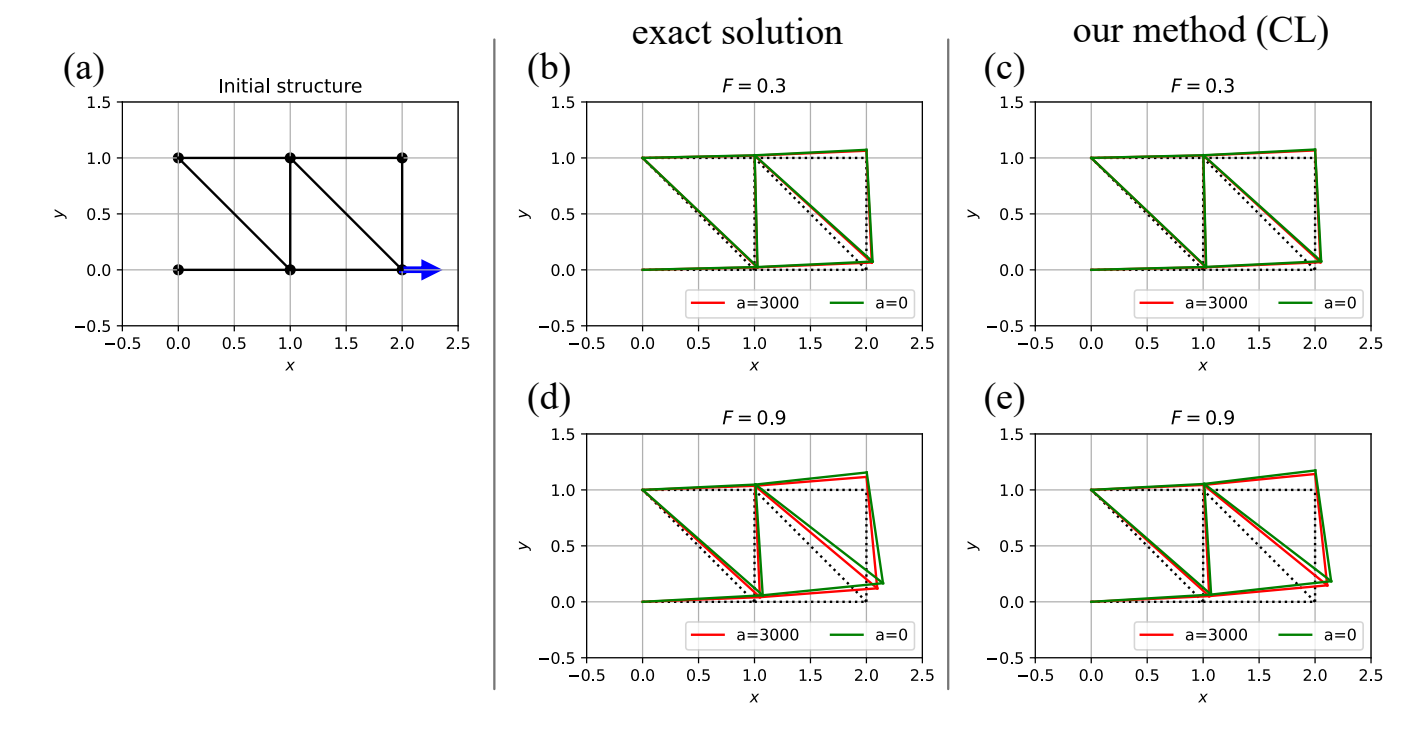


FIG. 4. Results for a two-dimensional truss system. (a) Target truss composed of masses (black points) and springs (black lines). External force is applied as blue arrow with strength F. (b) Exact deformation at F = 0.3 for linear springs (green) and nonlinear springs (red). (c) Obtained deformation using our method with Carleman linearization at F = 0.3. (d) Exact deformation at F = 0.9. (e) Obtained deformation using our method with Carleman linearization at F = 0.9.

all springs are at their natural lengths, we assume the *i*-th mass is located at fixed point  $(x_i, y_i)$ . We denote the displacement relative to this natural position as  $(u_i, v_i)$ . Our goal is to get the displacement of all the points when each external force  $(f_x^i, f_y^i)$  is applied to the *i*-th mass.

We begin with the internal potential energy, which is the sum of internal energy of all springs in G. Using the same nonlinear spring as in Eq. (4), the internal energy  $U_{i,j}$  of the spring (i,j) is

$$U_{ij} = \frac{k}{2} (\Delta L_{i,j})^2 + \frac{a}{4} (\Delta L_{i,j})^4, \tag{25}$$

where we denote the length of the spring  $\Delta L_{i,j}$ .  $\Delta L_{i,j}$  can be expressed as

$$\Delta L_{i,j} = \sqrt{(x+u)^2 + (y+v)^2} - L_0, \tag{26}$$

where we define  $x = x_i - x_j$ ,  $y = y_i - y_j$ ,  $u = u_i - u_j$ ,  $v = v_i - v_j$  and  $L_0 = \sqrt{x^2 + y^2}$  for simplicity.

We approximate  $U_{i,j}$  to a polynomial function for modeling purpose, similar to taking a first-order approximation for infinitesimal deformations. Note that this polynomial approximation is **not** related to exact linearization methods, such as Carleman linearization. Since the energy of this nonlinear spring includes a quartic term (related to a), we use a fourth-order polynomial approximation to maintain material nonlinearity. Then the en-

ergy of spring is approximated as  $\hat{U}_{i,j} =$ 

$$\frac{k}{2} \left( \frac{l_1^2}{L_0^2} + \frac{l_1 l_2}{L_0^2} - \frac{l_1^3}{L_0^4} + \frac{l_2^2}{4L_0^2} - \frac{3l_1^2 l_2}{2L_0^4} + \frac{5l_1^4}{4L_0^6} \right) + \frac{al_1^4}{4L_0^4},\tag{27}$$

where we denote  $l_1 = ux + vy$  and  $l_2 = u^2 + v^2$ . The proof is shown in Appendix D. It is important to note that  $l_1, l_2$  only have linear and quadratic terms with respect to the variables, respectively.

Including the energy of the external forces, the total potential energy of the system U is therefore

$$U = \sum_{(i,j)\in G} \hat{U}_{ij} - \sum_{i=1}^{N} (f_x^i u_i + f_y^i v_i).$$
 (28)

Then we can calculate the equilibrium displacement  $\{(u_i, v_i)\}$  satisfies  $\nabla_{u_i} U = \nabla_{v_i} U = 0$  using our method.

We solved the equilibrium displacement of the truss with the initial structure shown in Fig. 4(a). All springs use k=10 and a=3000, consistent with the previous examples. To confirm nonlinear effects, we also consider the purely linear case k=10 and a=0. In this initial structure, six masses (black dots) are exists but the masses at (0,0) and (0,1) are fixed in position. So these two masses are excluded from the state vector. An external force is applied only at the node located at (2,0) with the force vector (F,0) (blue arrow). We use F=0.3 and

0.9 for this experiment. The nonlinear time evolution equations obtained by our method is exactly linearized by Carleman linearization, and truncated at the order P=5. We got the solutions by numerically integrating the obtained truncated time evolution.

Fig. 4(c) and 4(e) shows the obtained results for F=0.3 and 0.9, respectively. For comparison, we calculate the exact solution by minimizing the total potential Eq. (28) using classical nonlinear solver. Fig. 4(b) and 4(e) shows the exact solution in for F=0.3 and 0.9, respectively. In these four figures, the linear case (k=10,a=0) is plotted in green, and the nonlinear case (k=10,a=3000) in red.

In F=0.3, the external force is sufficiently small that the response remains in the linear. We can confirmed this by the fact that exact solutions for the linear (green) and nonlinear (red) case in Fig.4 (b) coincide. The obtained results using our method in Fig. 4(c) match this exact solutions correctly for both the linear and nonlinear cases. Thus, it is clear that when displacements remain in linear region, our method predicts the response to the external force accurately.

For F=0.9, the exact solution in Fig. 4(d) shows that the nonlinear case (red) exhibits reduced displacements relative to the linear case (green). Fig. 4(e) shows that our method successfully reproduce these reduced displacements. The suppression of the displacements, however, is somewhat milder than in the exact solutions. This is due to the errors introduced by Carleman linearization, as confirmed by the first and second numerical experiments.

## IV. CONCLUSION

In this study, we presented a novel fault-tolerant quantum computing (FTQC) algorithm for solving nonlinear equilibrium equations derived from variational principles. The central concept of the proposed approach is the reformulation of nonlinear equilibrium conditions into nonlinear time-evolution equations, which are then rigorously linearized into infinite-dimensional linear dynamics via Carleman or Pivot State Carleman (PSC) linearization. While practical implementations necessitate finite-dimensional truncation, our results demonstrate that even truncated versions of the algorithm can successfully capture the nonlinear characteristics of the original equations. The accurate prediction of nonlinear deformation in a two-dimensional truss system using our

method represents a significant advancement in the practical application of quantum accelerations to nonlinear systems.

We further assessed the quantum resource requirements of the algorithm and showed that quantum computers can provide exponential memory savings compared to classical counterparts. The query complexity for computing the time evolution scales linearly with the evolution time t, and is independent of system size N. These properties underscore the potential of our algorithm to solve large-scale nonlinear equilibrium problems with substantially reduced computational resources.

The choice of linearization method plays a crucial role and must be tailored to the specific characteristics of the problem. Carleman linearization can suffer from divergence in strongly nonlinear regimes, an issue partially mitigated by the PSC approach. PSC benefits from selecting a pivot state close to the true solution, making it particularly suitable for systems where approximate solutions—such as those obtained by neglecting nonlinearity or external force directionality—can guide the initialization. Our structural analysis example demonstrates the effectiveness of this strategy, suggesting that improved divergence-mitigation techniques could enhance linear approximation quality across diverse nonlinear problems.

The evolution time required for accurate solution reconstruction is another critical factor and depends on both the system and the initial state. In the ideal case where the initial state coincides with the final solution, the required evolution time vanishes. This highlights the importance of incorporating prior knowledge and system-specific heuristics into initial state selection—paralleling the role of preconditioning in quantum linear system algorithms. We anticipate that the development of advanced "pre-initialization" strategies will further reduce computational costs.

Finally, the proposed algorithm is not restricted to nonlinear structural mechanics. It is applicable to a wide array of nonlinear equilibrium problems derived from variational principles, including those in fluid dynamics, electromagnetics, chemical kinetics, biological systems, and nonequilibrium thermodynamics. In particular, it may enable quantum acceleration in tasks such as stability analysis, reaction rate estimation, and complex system dynamics. We hope this work serves as a foundation for the development of more general-purpose quantum algorithms for tackling nonlinear variational problems across scientific disciplines.

<sup>[1]</sup> L. D. Landau and E. M. Lifshitz, Course of theoretical physics (Elsevier, 2013).

<sup>[2]</sup> R. P. Feynman, The principle of least action in quantum mechanics, in *Feynman's thesis—a new approach to quantum theory* (World Scientific, 2005) pp. 1–69.

<sup>[3]</sup> D. Hilbert, Die grundlagen der physik . (erste mit-

teilung.), Nachrichten von der Gesellschaft der Wissenschaften zu Göttingen, Mathematisch-Physikalische Klasse 1915, 395 (1915).

<sup>[4]</sup> E. Noether, Invariante variationsprobleme, in Gesammelte Abhandlungen-Collected Papers (Springer, 1983) pp. 231–239.

- [5] K. Washizu, Variational Methods in Elasticity and Plasticity. (Pergamon Press, 1968).
- [6] P. J. Morrison, Hamiltonian description of the ideal fluid, Reviews of modern physics 70, 467 (1998).
- [7] J. D. Jackson, Classical electrodynamics (John Wiley & Sons, 2021).
- [8] L. Landau, E. Lifshitz, and L. E. Reichl, Statistical physics, part 1 (1981).
- [9] E. Tadmor, A review of numerical methods for nonlinear partial differential equations, Bulletin of the American Mathematical Society 49, 507 (2012).
- [10] D. A. Knoll and D. E. Keyes, Jacobian-free newtonkrylov methods: a survey of approaches and applications, Journal of Computational Physics 193, 357 (2004).
- [11] S. De, Uncertainty quantification of locally nonlinear dynamical systems using neural networks, Journal of Computing in Civil Engineering 35, 04021009 (2021).
- [12] P. W. Shor, Algorithms for quantum computation: discrete logarithms and factoring, in *Proceedings 35th annual symposium on foundations of computer science* (Ieee, 1994) pp. 124–134.
- [13] L. K. Grover, A fast quantum mechanical algorithm for database search, in *Proceedings of the twenty-eighth an*nual ACM symposium on Theory of computing (1996) pp. 212–219.
- [14] N. Linden, A. Montanaro, and C. Shao, Quantum vs. classical algorithms for solving the heat equation, Communications in Mathematical Physics 395, 601 (2022).
- [15] P. C. Costa, S. Jordan, and A. Ostrander, Quantum algorithm for simulating the wave equation, Physical Review A 99, 012323 (2019).
- [16] A. W. Harrow, A. Hassidim, and S. Lloyd, Quantum algorithm for linear systems of equations, Physical review letters 103, 150502 (2009).
- [17] A. Gilyén, Y. Su, G. H. Low, and N. Wiebe, Quantum singular value transformation and beyond: exponential improvements for quantum matrix arithmetics, in *Pro*ceedings of the 51st annual ACM SIGACT symposium on theory of computing (2019) pp. 193–204.
- [18] P. C. Costa, D. An, Y. R. Sanders, Y. Su, R. Babbush, and D. W. Berry, Optimal scaling quantum linearsystems solver via discrete adiabatic theorem, PRX quantum 3, 040303 (2022).
- [19] Y. Subaşı, R. D. Somma, and D. Orsucci, Quantum algorithms for systems of linear equations inspired by adiabatic quantum computing, Physical review letters 122, 060504 (2019).
- [20] A. Montanaro and S. Pallister, Quantum algorithms and the finite element method, Physical Review A 93, 032324 (2016).
- [21] S. Sinha and P. Russer, Quantum computing algorithm for electromagnetic field simulation, Quantum Information Processing 9, 385 (2010).
- [22] B. D. Clader, B. C. Jacobs, and C. R. Sprouse, Preconditioned quantum linear system algorithm, Physical review letters 110, 250504 (2013).
- [23] D. W. Berry, A. M. Childs, A. Ostrander, and G. Wang, Quantum algorithm for linear differential equations with exponentially improved dependence on precision, Communications in Mathematical Physics 356, 1057 (2017).
- [24] D. W. Berry, High-order quantum algorithm for solving linear differential equations, Journal of Physics A: Mathematical and Theoretical 47, 105301 (2014).
- [25] A. Engel, G. Smith, and S. E. Parker, Quantum algo-

- rithm for the vlasov equation, Physical Review A 100, 062315 (2019).
- [26] I. Novikau, E. Startsev, and I. Y. Dodin, Quantum signal processing for simulating cold plasma waves, Physical Review A 105, 062444 (2022).
- [27] K. Miyamoto, S. Yamazaki, F. Uchida, K. Fujisawa, and N. Yoshida, Quantum algorithm for the vlasov simulation of the large-scale structure formation with massive neutrinos, Physical Review Research 6, 013200 (2024).
- [28] A. Suau, G. Staffelbach, and H. Calandra, Practical quantum computing: Solving the wave equation using a quantum approach, ACM Transactions on Quantum Computing 2, 1 (2021).
- [29] R. Babbush, D. W. Berry, R. Kothari, R. D. Somma, and N. Wiebe, Exponential quantum speedup in simulating coupled classical oscillators, Physical Review X 13, 041041 (2023).
- [30] J. Gonzalez-Conde, Á. Rodríguez-Rozas, E. Solano, and M. Sanz, Efficient hamiltonian simulation for solving option price dynamics, Physical Review Research 5, 043220 (2023).
- [31] S. Jin, N. Liu, and Y. Yu, Quantum simulation of partial differential equations via schrodingerisation: technical details, arXiv preprint arXiv:2212.14703 (2022).
- [32] D. An, J.-P. Liu, and L. Lin, Linear combination of hamiltonian simulation for nonunitary dynamics with optimal state preparation cost, Physical Review Letters 131, 150603 (2023).
- [33] D. An, A. M. Childs, and L. Lin, Quantum algorithm for linear non-unitary dynamics with near-optimal dependence on all parameters, arXiv preprint arXiv:2312.03916 (2023).
- [34] J.-P. Liu, H. Ø. Kolden, H. K. Krovi, N. F. Loureiro, K. Trivisa, and A. M. Childs, Efficient quantum algorithm for dissipative nonlinear differential equations, Proceedings of the National Academy of Sciences 118, e2026805118 (2021).
- [35] A. Engel, G. Smith, and S. E. Parker, Linear embedding of nonlinear dynamical systems and prospects for efficient quantum algorithms, Physics of Plasmas 28, 062305 (2021).
- [36] J.-P. Liu, D. An, D. Fang, J. Wang, G. H. Low, and S. Jordan, Efficient quantum algorithm for nonlinear reaction-diffusion equations and energy estimation, Communications in Mathematical Physics 404, 963 (2023).
- [37] P. Costa, P. Schleich, M. E. Morales, and D. W. Berry, Further improving quantum algorithms for nonlinear differential equations via higher-order methods and rescaling, arXiv preprint arXiv:2312.09518 (2023).
- [38] I. Joseph, Koopman-von neumann approach to quantum simulation of nonlinear classical dynamics, Physical Review Research 2, 043102 (2020).
- [39] S. Jin, N. Liu, and Y. Yu, Time complexity analysis of quantum algorithms via linear representations for nonlinear ordinary and partial differential equations, Journal of Computational Physics 487, 112149 (2023).
- [40] H. Krovi, Improved quantum algorithms for linear and nonlinear differential equations, Quantum 7, 913 (2023).
- [41] K. Endo and K. Z. Takahashi, Divergence-free algorithms for solving nonlinear differential equations on quantum computers, arXiv preprint arXiv:2411.16233 (2024).
- [42] C. Xue, X.-F. Xu, Y.-C. Wu, and G.-P. Guo, Quantum al-

gorithm for solving a quadratic nonlinear system of equations, Physical Review A 106, 032427 (2022).

- [43] N. A. Nghiem and T.-C. Wei, Quantum algorithm for solving nonlinear algebraic equations, arXiv preprint arXiv:2404.03810 (2024).
- [44] C. Sanavio, R. Scatamacchia, C. de Falco, and S. Succi, Three carleman routes to the quantum simulation of classical fluids, Physics of Fluids 36 (2024).
- [45] W. Itani and S. Succi, Analysis of carleman linearization of lattice boltzmann, Fluids 7, 24 (2022).
- [46] W. Itani, K. R. Sreenivasan, and S. Succi, Quantum algorithm for lattice boltzmann (qalb) simulation of incompressible fluids with a nonlinear collision term, Physics of Fluids 36 (2024).
- [47] G. H. Low and I. L. Chuang, Optimal hamiltonian simulation by quantum signal processing, Physical review letters 118, 010501 (2017).
- [48] G. H. Low and I. L. Chuang, Hamiltonian simulation by qubitization, Quantum 3, 163 (2019).
- [49] E. A. Coddington and N. Levinson, Theory of ordinary differential equations (McGraw-Hill New York, 1955).

# Appendix A: A simple proof for the arrival to the solution

Consider the time evolution equations

$$\frac{d\mathbf{u}}{dt} = -\mathbf{f}(\mathbf{u}). \tag{A1}$$

as shown in Eq. 3. f satisfies

$$f(u) = \nabla_u U \tag{A2}$$

where (1)  $\nabla_{\boldsymbol{u}}U$  is locally Lipschitz continuous in anywhere, (2)  $U(\boldsymbol{u}) \to \infty$  when  $\|\boldsymbol{u}\| \to \infty$ .

From the Picard–Lindelöf theorem[49], since  $\boldsymbol{f}$  is locally Lipschitz continuous, the trajectory of  $\boldsymbol{u}(t)$  is unique for any initial state  $\boldsymbol{u}(0)$ . The condition locally Lipschitz continuous is also implies that U is continuous function. Continuity of U and  $U(\boldsymbol{u}) \to \infty$  when  $\|\boldsymbol{u}\|$  means U has global minimums.

Since

$$\frac{dU}{dt}(\boldsymbol{u}) = -\boldsymbol{\nabla}_{\boldsymbol{u}}U \cdot \frac{d\boldsymbol{u}}{dt} = -\|\boldsymbol{\nabla}_{\boldsymbol{u}}U\|^2 \le 0, \quad (A3)$$

U(t) decreases monotonically. Combined with the fact U has a global minimum value, the limit of  $U(t \to \infty)$  exists and its value is finite. This implies that

$$\int_{t=0}^{\infty} \|\nabla_{\boldsymbol{u}} U\|^2 = U(t=0) - U(t \to \infty) \tag{A4}$$

is finite, resulting

$$\lim_{t \to \infty} \| \nabla_{\boldsymbol{u}} U \| = 0. \tag{A5}$$

# Appendix B: The equivalence of Eq. (13) and Eq. (14)

We expand the the right side of following equation

$$\frac{d\mathbf{u}}{dt} = F_0 \mathbf{u}^{\otimes 0} + F_1 \mathbf{u}^{\otimes 1} + F_3 \mathbf{u}^{\otimes 3}$$
 (B1)

(identical to Eq. (14)) element by element and verify that it matches Eq. (13).

For the first term, we got

$$(F_0 \boldsymbol{u}^{\otimes 0})_i = (\boldsymbol{b})_i = b_i. \tag{B2}$$

For the second term, we got

$$(F_{1}\boldsymbol{u}^{\otimes 1})_{i}$$

$$=k((S+S^{T}-2I)\boldsymbol{u})_{i}$$

$$=k((S\boldsymbol{u})_{i}+(S^{T}\boldsymbol{u})_{i}-2(\boldsymbol{u})_{i}$$

$$=k(u_{i+1}+u_{i-1}-2u_{i})$$

$$=-k[(u_{i}-u_{i-1})+(u_{i}-u_{i-1})].$$
(B3)

For the third term, we got

$$(F_3 \mathbf{u}^{\otimes 3})_i$$

$$= (aV \{ (S^T - I)^{\otimes 3} - (I - S)^{\otimes 3} \} \mathbf{u}^{\otimes 3})_i$$

$$= a (V(S^T \mathbf{u} - \mathbf{u})^{\otimes 3})_i - a (V(\mathbf{u} - S\mathbf{u})^{\otimes 3})_i$$

$$= a[(S^T \mathbf{u} - \mathbf{u})_i]^3 - a[(\mathbf{u} - S\mathbf{u})_i]^3$$

$$= -a [(u_i - u_{i-1})^3 + (u_i - u_{i-1})^3]$$
(B4)

Therefore, the sum of the three term is equal to Eq. (13).

## Appendix C: Estimated query complexity of Eq. (22)

We consider the case we have the block encoding of  $A/\alpha$ , where  $\alpha = ||A||_2$ . In this case, since the query complexity for simulating Eq. (22) grows as  $\mathcal{O}(\alpha t + \ln(1/\epsilon))$ , we have to estimate the size of  $\alpha = ||A||_2$  with given P, a, k, b.

First, we get the upper bound

$$||A||_{2}^{2} \leq \sum_{p=1}^{P} ||C(F_{0}, p)||_{2}^{2} + \sum_{p=1}^{P} ||C(F_{1}, p)||_{2}^{2} + \sum_{p=1}^{P-2} ||C(F_{3}, p)||_{2}^{2}, \quad (C1)$$

where we use the inequality  $||[X \ Y]||_2^2 \le ||X||_2^2 + ||Y||_2^2$  multiple times.

Second, we evaluate the upper bound of spectral norm

of C(F, p) as

$$||C(F,p)|| = \left\| \sum_{v=0}^{p-1} \underbrace{I \otimes \cdots \otimes I}_{v \text{ times}} \otimes F \otimes \underbrace{I \otimes \cdots \otimes I}_{p-1-v \text{ times}} \right\|_{2}$$

$$\leq \sum_{v=0}^{p-1} \left\| \underbrace{I \otimes \cdots \otimes I}_{v \text{ times}} \otimes F \otimes \underbrace{I \otimes \cdots \otimes I}_{p-1-v \text{ times}} \right\|_{2}$$

$$= \sum_{v=0}^{p-1} ||F||_{2} = p||F||_{2}, \qquad (C2)$$

where we used the inequality  $||X + Y||_2 \le ||X||_2 + ||Y||_2$  and the equality  $||X \otimes Y||_2 = ||X||_2 ||Y||_2$ . Thus, substituting Eq. (C1) to Eq. (C2), we get

$$||A||_{2}^{2} \leq \sum_{p=1}^{P} p^{2} ||F_{0}||_{2}^{2} + \sum_{p=1}^{P} p^{2} ||F_{1}||_{2}^{2} + \sum_{p=1}^{P-2} p^{2} ||F_{3}||_{2}^{2}.$$
  
$$\leq P^{3} (||F_{0}||_{2}^{2} + ||F_{1}||_{2}^{2} + ||F_{3}||_{2}^{2})$$
(C3)

We also evaluate the upper bound of the spectral norm of  $F_0, F_1, F_3$  as follows:

$$||F_0|| = ||\boldsymbol{b}|| \tag{C4}$$

$$||F_1|| = ||k(S + S^T - 2I)|| = k||S + S^T - 2I|| \le 4k.$$
 (C5)

$$||F_3|| = ||aV\{(S^T - I)^{\otimes 3} - (I - S)^{\otimes 3}\}|| = a||V\{(S^T - I)^{\otimes 3} - (I - S)^{\otimes 3}\}|| \le 2\sqrt{10}a.$$
 (C6)

Finally, substituting Eq. (C4-6) into Eq. (C3), we get

$$||A||_2^2 \le P^3(||\mathbf{b}||^2 + 16k^2 + 40a^2)$$
 (C7)

and, therefore, we get the order of  $||A||_2$  as

$$||A||_2 = \mathcal{O}(P^{3/2}(||\mathbf{b}|| + k + a)).$$
 (C8)

This immediately lead to Eq. (23).

## Appendix D: Derivation of the energy model of two-dimensional nonlinear spring Eq. (27)

The energy of the spring is defined as

$$U_{ij} = \frac{k}{2} (\Delta L_{i,j})^2 + \frac{a}{4} (\Delta L_{i,j})^4,$$
 (D1)

where

$$\Delta L_{i,j} = \sqrt{(x+u)^2 + (y+v)^2} - L_0$$
 (D2)

is the extension of the spring. We rewrite this spring extension as

$$\Delta L_{i,j} = L_0 \left( \sqrt{1 + \frac{2(ux + vy) + (x^2 + y^2)}{L_0^2}} - 1 \right)$$
(D3)  
=  $L_0 \left( \sqrt{1 + l} - 1 \right)$ , (D4)

where we define  $l = (2l_1 + l_2)/L_0^2$ ,  $l_1 = ux + vy$  and  $l_2 = x^2 + y^2$ .

Since the Taylor expansion of the function  $\sqrt{1+p}$  is

$$\sqrt{1+p} = 1 + \frac{1}{2}p - \frac{1}{8}p^2 + \frac{1}{16}p^3 - \frac{5}{128}p^4 + \cdots,$$
 (D5)

the spring extension is approximated to

$$\Delta L_{i,j} = L_0 \left( \frac{1}{2} l - \frac{1}{8} l^2 + \frac{1}{16} l^3 - \frac{5}{128} l^4 + \dots \right). \quad (D6)$$

Substituting this relation into Eq. (D1), we get

$$U_{ij} = \frac{kL_0^2}{2} \left( \frac{1}{2}l - \frac{1}{8}l^2 + \frac{1}{16}l^3 + \cdots \right)^2$$

$$+ \frac{aL_0^4}{4} \left( \frac{1}{2}l - \frac{1}{8}l^2 + \frac{1}{16}l^3 + \cdots \right)^4$$

$$= \frac{k}{2} \left( \frac{l_1^2}{L_0^2} + \frac{l_1l_2}{L_0^2} - \frac{l_1^3}{L_0^4} + \frac{l_2^2}{4L_0^2} - \frac{3l_1^2l_2}{2L_0^4} + \frac{5l_1^4}{4L_0^6} \right)$$

$$+ \frac{al_1^4}{4l_0^4} + \mathcal{O}((u+v)^5).$$
(D10)

Ignoring terms of order higher than 4, therefore, we obtained the following energy model  $\hat{U}_{ij}$  =

$$\frac{k}{2} \left( \frac{l_1^2}{L_0^2} + \frac{l_1 l_2}{L_0^2} - \frac{l_1^3}{L_0^4} + \frac{l_2^2}{4L_0^2} - \frac{3l_1^2 l_2}{2L_0^4} + \frac{5l_1^4}{4L_0^6} \right) + \frac{al_1^4}{4L_0^4}. \tag{D11}$$